

Electronic Supplementary Information

to

2-Formylphenoxyacetic Acid Schiff Bases: A Promising Ligand Scaffold for Readily Available Trigonal Prismatic Co(II) Single-Ion Magnets

Kamil Kotrle,^a Ivan Nemeč,^a Peter Antal,^a Kamila Petrželová,^a Erik Čižmár,^b and Radovan Herchel^{*a}

^a Department of Inorganic Chemistry, Faculty of Science, Palacký University, 17. listopadu 12, CZ-771 46 Olomouc, Czech Republic.

^b Institute of Physics, Faculty of Science, P.J. Šafárik University in Košice, Park Angelinum 9, SK-041 54 Košice, Slovakia

Figure S1. FTIR spectra of studied compounds 1-3 and 5-6	3
Figure S2. The experimental and calculated PXRD patterns for studied compounds.	4
Figure S3. Deviation of prepared complexes from minimal distortion pathway between octahedron and trigonal prism calculated by SHAPE.	5
Figure S4. Correlation between index τ_6 and CSM deviations from octahedron and trigonal prism for studied complexes	5
Figure S5. A perspective view illustrating O–H···O hydrogen bonding (black dashed lines) in the crystal structures of 1 (A), 3 (B), 4 (C) and 5 (D). The donor···acceptor distances of the depicted hydrogen bonds are as follows (in Å): 1 , $d(\text{O7}\cdots\text{O5}) = 2.765(2)$, 3 , $d(\text{O7}\cdots\text{O1}) = 2.745(2)$, 4 , $d(\text{O7}\cdots\text{O5}) = 2.842(6)$, $d(\text{O8}\cdots\text{O6}) = 2.752(3)$, 5 , $d(\text{O6}\cdots\text{O13}) = 2.691(3)$	6
Figure S6. DC magnetic data with experimental data points and theoretical fit of dependence of magnetic moment on temperature and magnetization on magnetic field for 1	7
Figure S7. DC magnetic data with experimental data points and theoretical fit of dependence of magnetic moment on temperature and magnetization on magnetic field for 2	7
Figure S8. DC magnetic data with experimental data points and theoretical fit of dependence of magnetic moment on temperature and magnetization on magnetic field for 3	7
Figure S9. DC magnetic data with experimental data points and theoretical fit of dependence of magnetic moment on temperature and magnetization on magnetic field for 5	8
Figure S10. DC magnetic data with experimental data points and theoretical fit of dependence of magnetic moment on temperature and magnetization on magnetic field for 6	8
Figure S11. AC magnetic data and relaxation time fit for 1 , shown are dependences of in-phase and out-of-phase susceptibilities on frequency (upper left and right), Cole-Cole diagram (lower left) and fit of relaxation time (lower right).	9
Figure S12. AC magnetic data and relaxation time fit for 2 , shown are dependences of in-phase and out-of-phase susceptibilities on frequency (upper left and right), Cole-Cole diagram (lower left) and fit of relaxation time (lower right).	10

Figure S13. AC magnetic data and relaxation time fit for 3 , shown are dependences of in-phase and out-of-phase susceptibilities on frequency (upper left and right), Cole-Cole diagram (lower left) and fit of relaxation time (lower right).	11
Figure S14. AC magnetic data and relaxation time fit for 5 , shown are dependences of in-phase and out-of-phase susceptibilities on frequency (upper left and right), Cole-Cole diagram (middle left) and fits of relaxation time (middle right and lower).	12
Figure S15: AC magnetic data for 6 , shown are dependences of in-phase and out-of-phase susceptibilities on frequency (upper left and right) and Cole-Cole diagram (lower).	13
Figure S16: AC magnetic data for 1Zn , shown are dependences of in-phase and out-of-phase susceptibilities on frequency for various temperatures and $B = 0.1$ T (a and b), Cole-Cole diagram for various temperatures and $B = 0.1$ T (c), dependences of in-phase and out-of-phase susceptibilities on frequency for various magnetic fields and $T = 2$ K (d and e), Cole-Cole diagram for various frequency for various magnetic fields and $T = 2$ K (f), and fits of relaxation time dependent on temperature (g) and magnetic field (h).	15
Figure S17: Thermal evolution of the powder X-band EPR spectra of 1 , 1Zn , 2 , 3 , 5 , and 6	16
Figure S18. Simulations of the powder X-band EPR spectra of 1 , 1Zn , 3 , 5 , and 6 obtained at 2.3 K using effective $S_{\text{eff}} = 1/2$ Hamiltonian and spin Hamiltonian models.	17
Figure S19. SINGLE_ANISO description of magnetic moment matrix elements between Kramers doublets for studied complexes.	19
Figure S20. The comparison of structural parameter τ_g calculated for 1-6 using X-ray data and data from DFT calculations.	19
Table S1. Detailed information about crystallographic experiments regarding 1-6	20
Table S2: Uncertainties of best-fitted parameters from DC magnetic measurements (Table 3) ..	21
Table S3. AC magnetic data fit parameters for 1	21
Table S4. AC magnetic data fit parameters for 2	22
Table S5. AC magnetic data fit parameters for 3	22
Table S6. AC magnetic data fit parameters for 5	23
Table S7. AC magnetic data fit parameters for 1Zn	23
Table S8. CASSCF/NEVPT2 calculated g -factors of Kramers doublets for studied complexes 1-6	23
Table S9. Selected structural parameters along with CSM and τ_g shape analysis of DFT optimized molecular structures for 1-6 with the help of B3LYP functional	24
Table S10. The comparison of Continuous Shape Measures for complexes reported in CSD. ^a	24

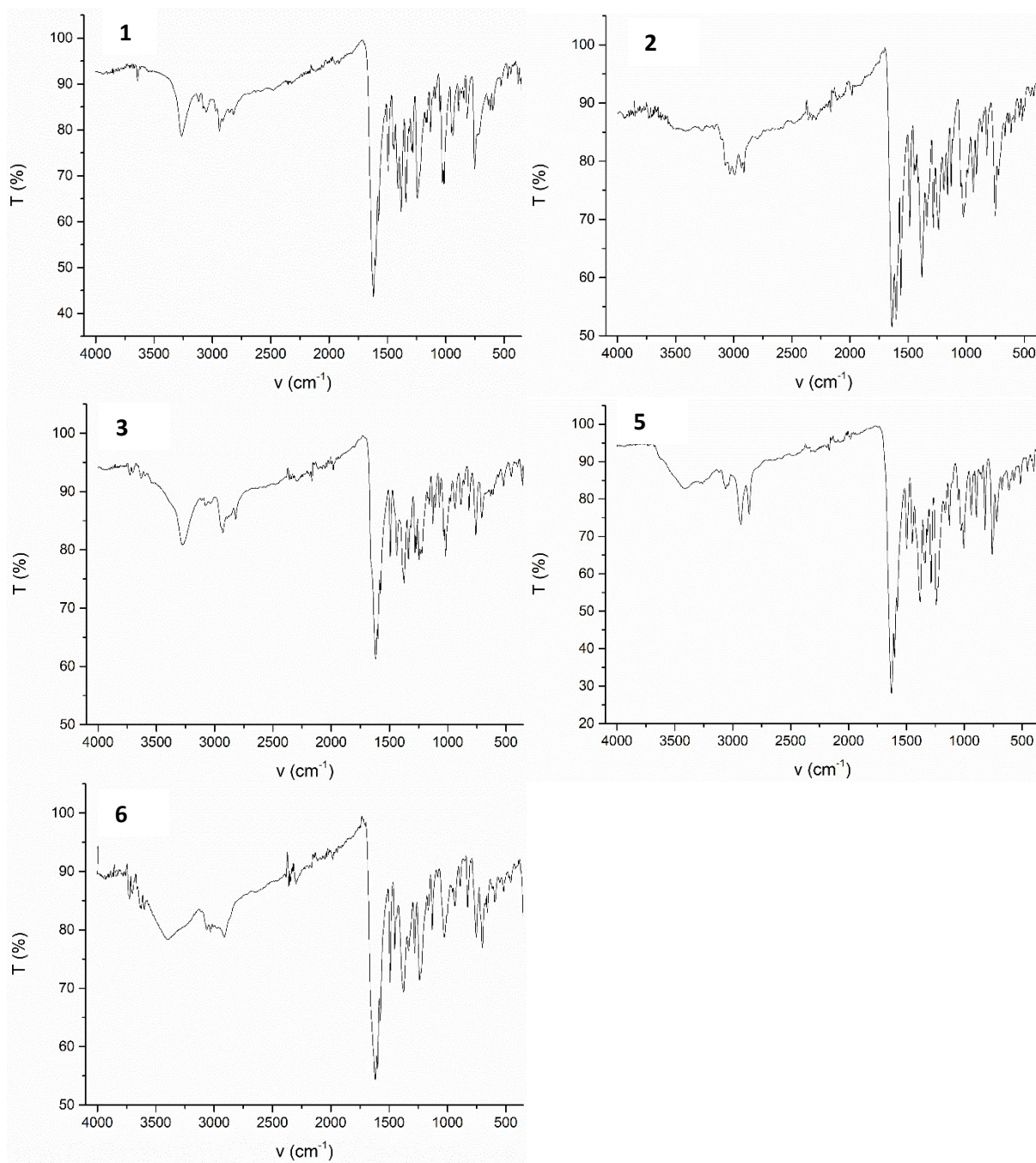


Figure S1. FTIR spectra of studied compounds **1-3** and **5-6**.

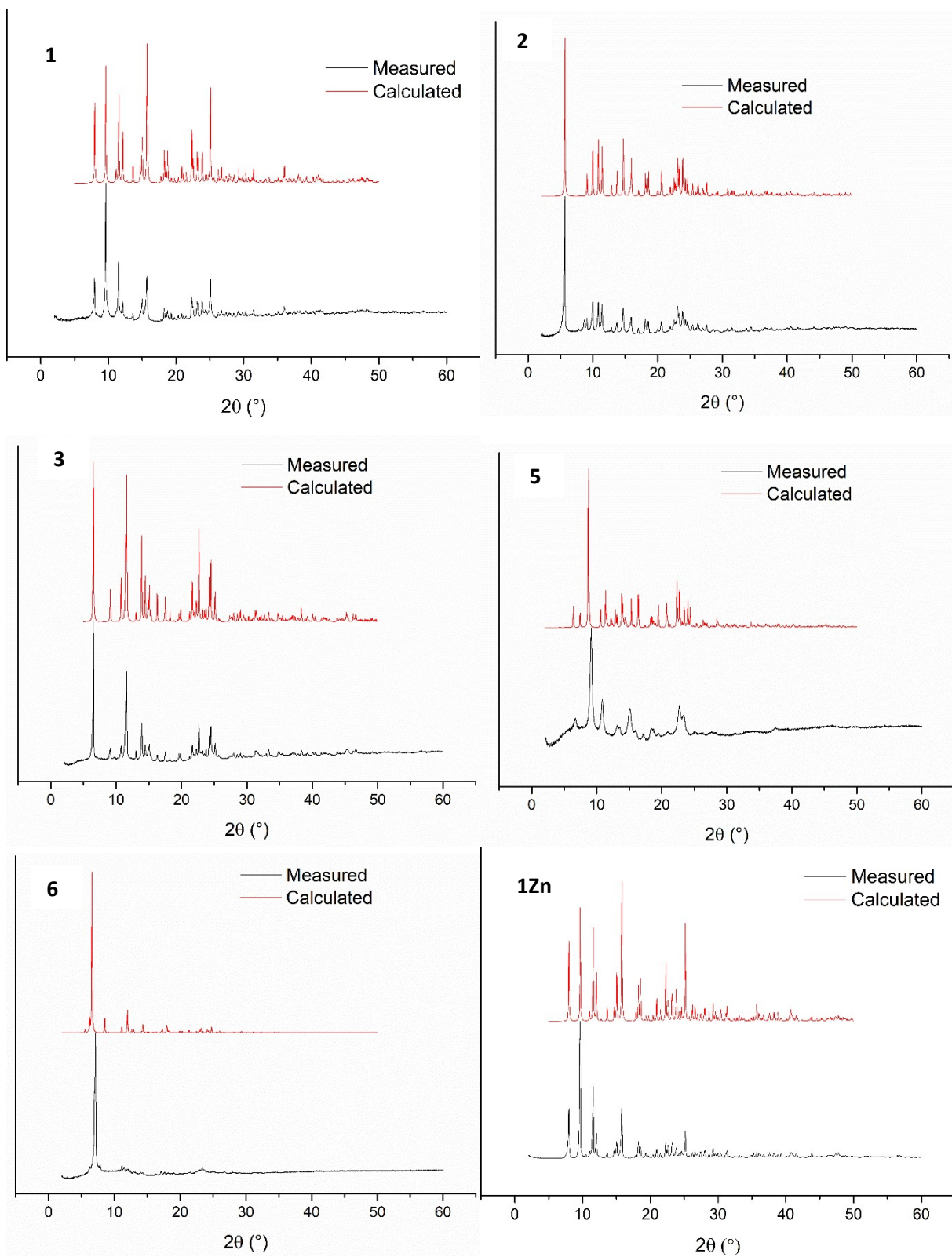


Figure S2. The experimental and calculated PXR D patterns for studied compounds.

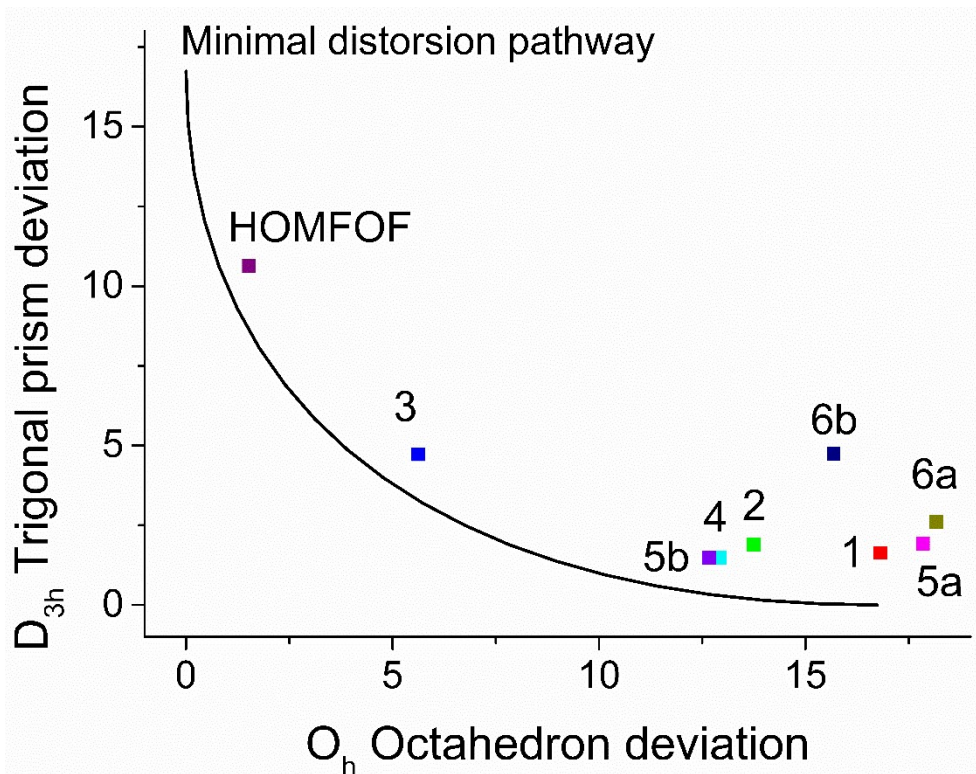


Figure S3. Deviation of prepared complexes from minimal distortion pathway between octahedron and trigonal prism calculated by SHAPE.

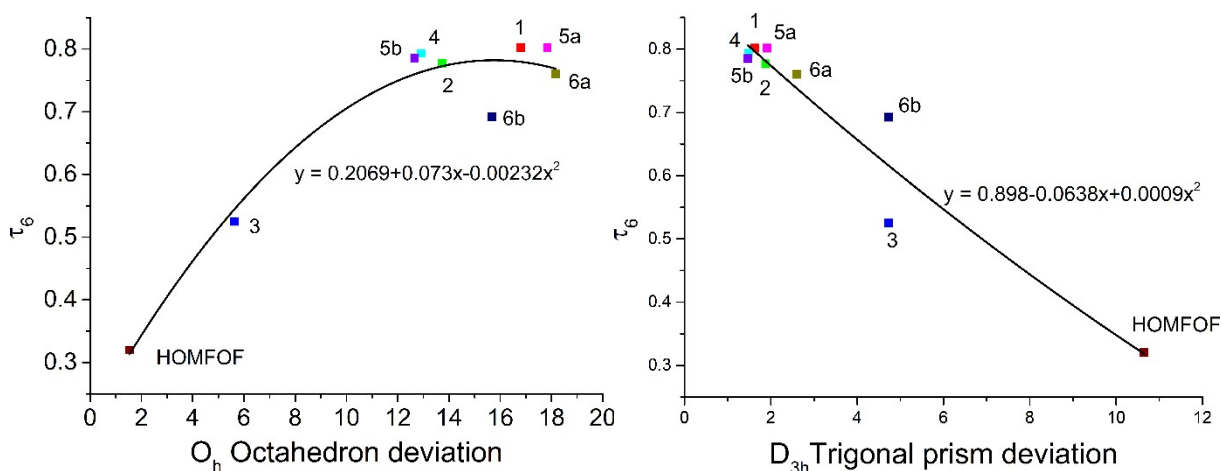


Figure S4. Correlation between index τ_6 and CSM deviations from octahedron and trigonal prism for studied complexes

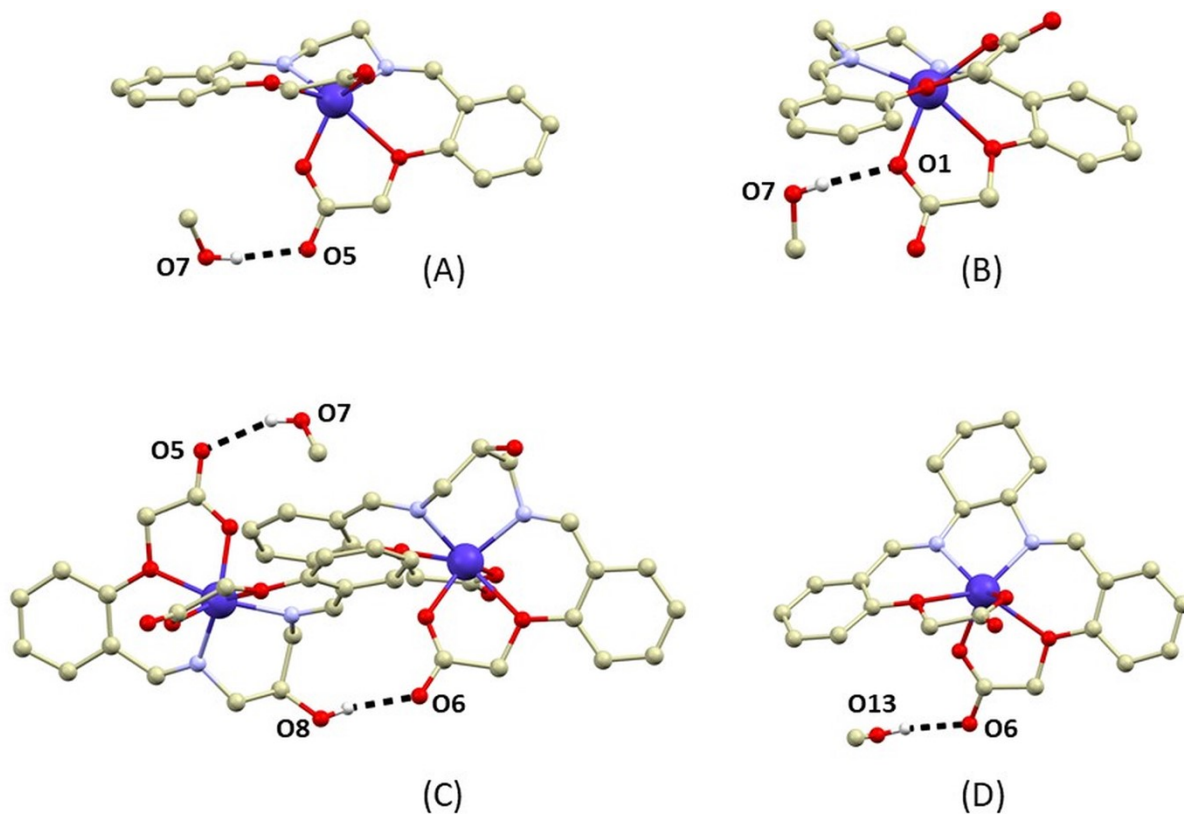


Figure S5. A perspective view illustrating O–H···O hydrogen bonding (black dashed lines) in the crystal structures of **1** (A), **3** (B), **4** (C) and **5** (D). The donor···acceptor distances of the depicted hydrogen bonds are as follows (in Å): **1**, $d(\text{O7}\cdots\text{O5}) = 2.765(2)$, **3**, $d(\text{O7}\cdots\text{O1}) = 2.745(2)$, **4**, $d(\text{O7}\cdots\text{O5}) = 2.842(6)$, $d(\text{O8}\cdots\text{O6}) = 2.752(3)$, **5**, $d(\text{O6}\cdots\text{O13}) = 2.691(3)$.

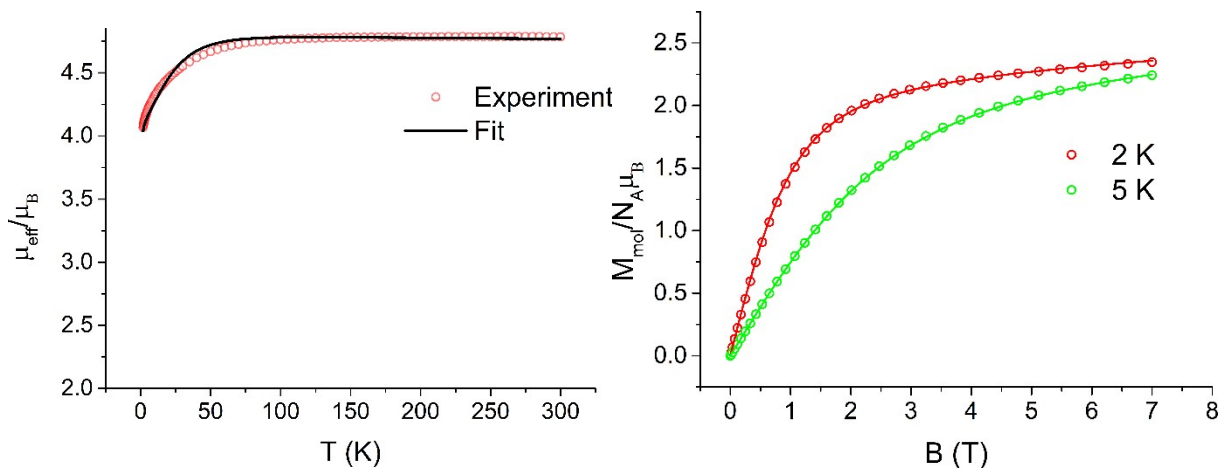


Figure S6. DC magnetic data with experimental data points and theoretical fit of dependence of magnetic moment on temperature and magnetization on magnetic field for **1**.

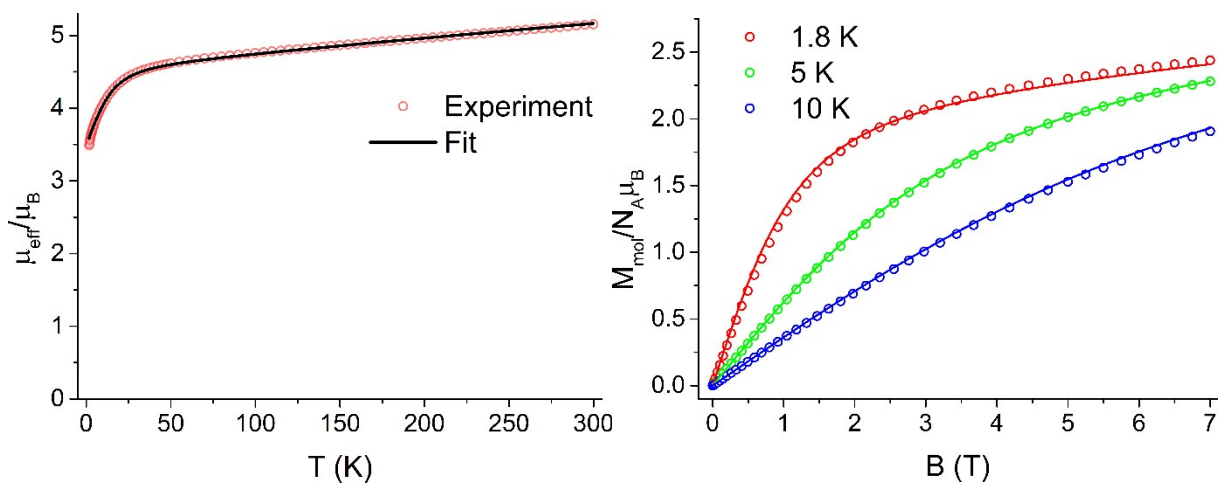


Figure S7. DC magnetic data with experimental data points and theoretical fit of dependence of magnetic moment on temperature and magnetization on magnetic field for **2**.

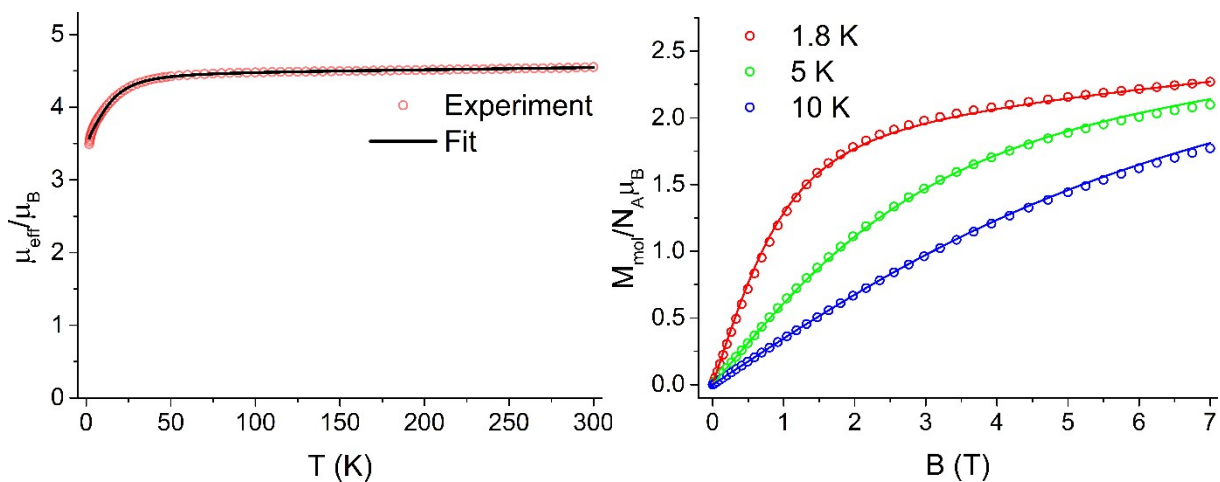


Figure S8. DC magnetic data with experimental data points and theoretical fit of dependence of magnetic moment on temperature and magnetization on magnetic field for **3**.

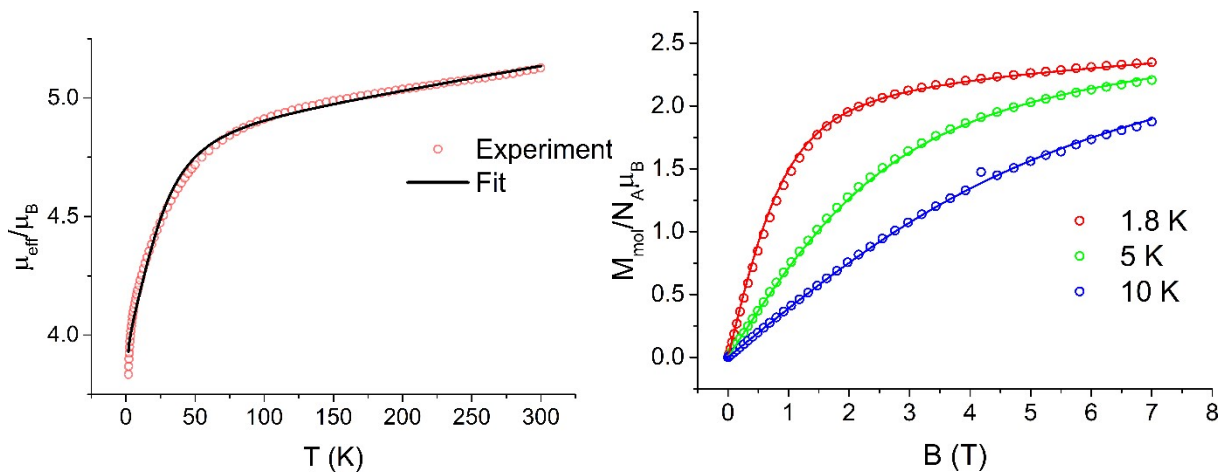


Figure S9. DC magnetic data with experimental data points and theoretical fit of dependence of magnetic moment on temperature and magnetization on magnetic field for 5.

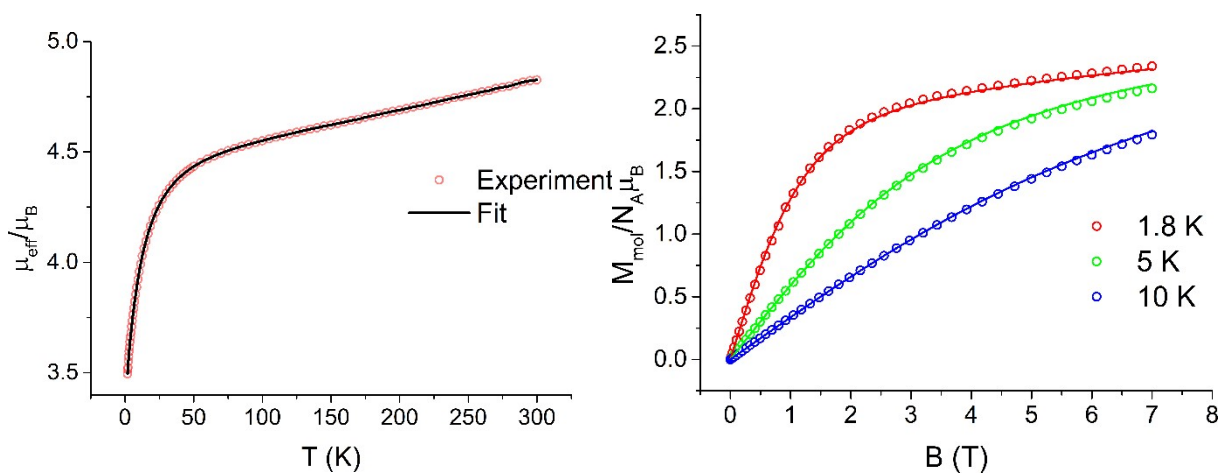


Figure S10. DC magnetic data with experimental data points and theoretical fit of dependence of magnetic moment on temperature and magnetization on magnetic field for 6.

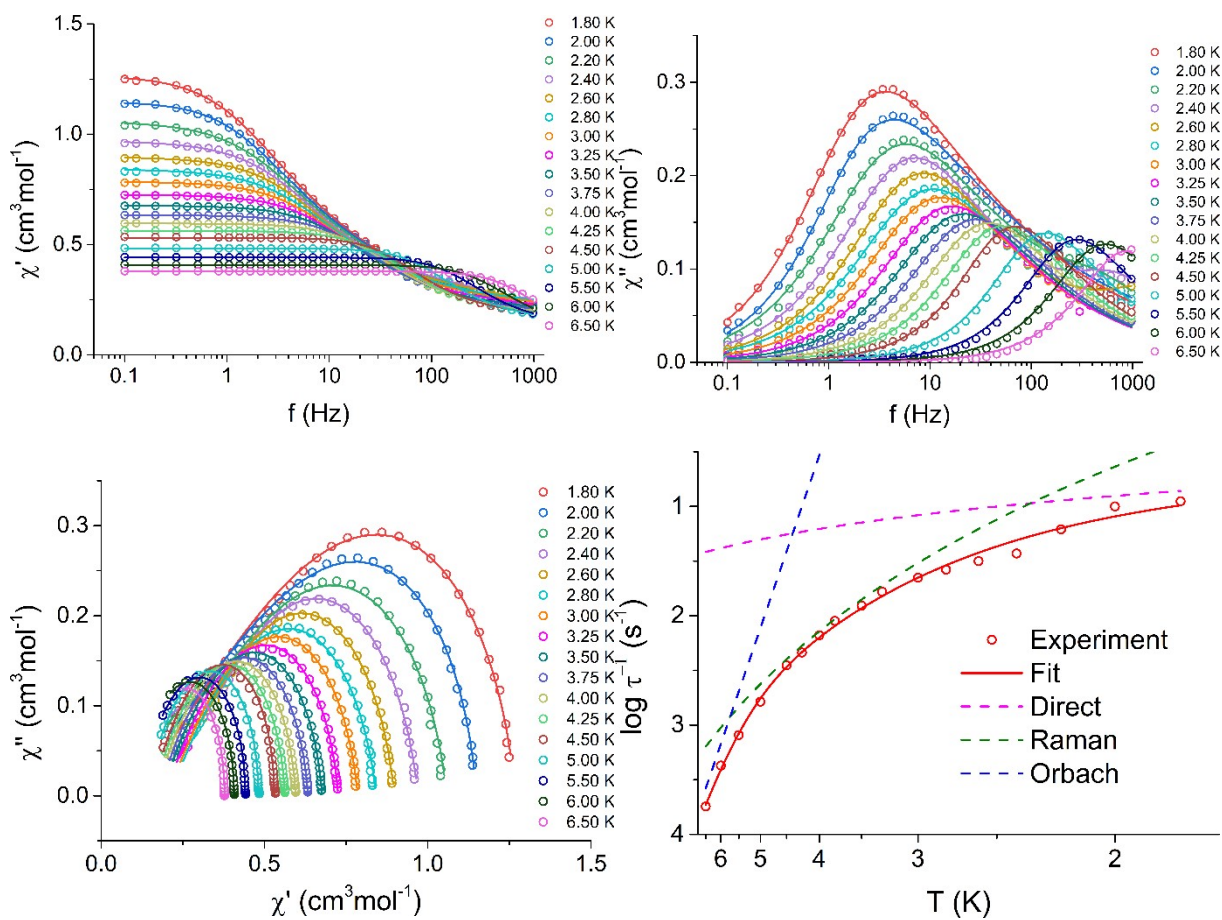


Figure S11. AC magnetic data and relaxation time fit for **1**, shown are dependences of in-phase and out-of-phase susceptibilities on frequency (upper left and right), Cole-Cole diagram (lower left) and fit of relaxation time (lower right).

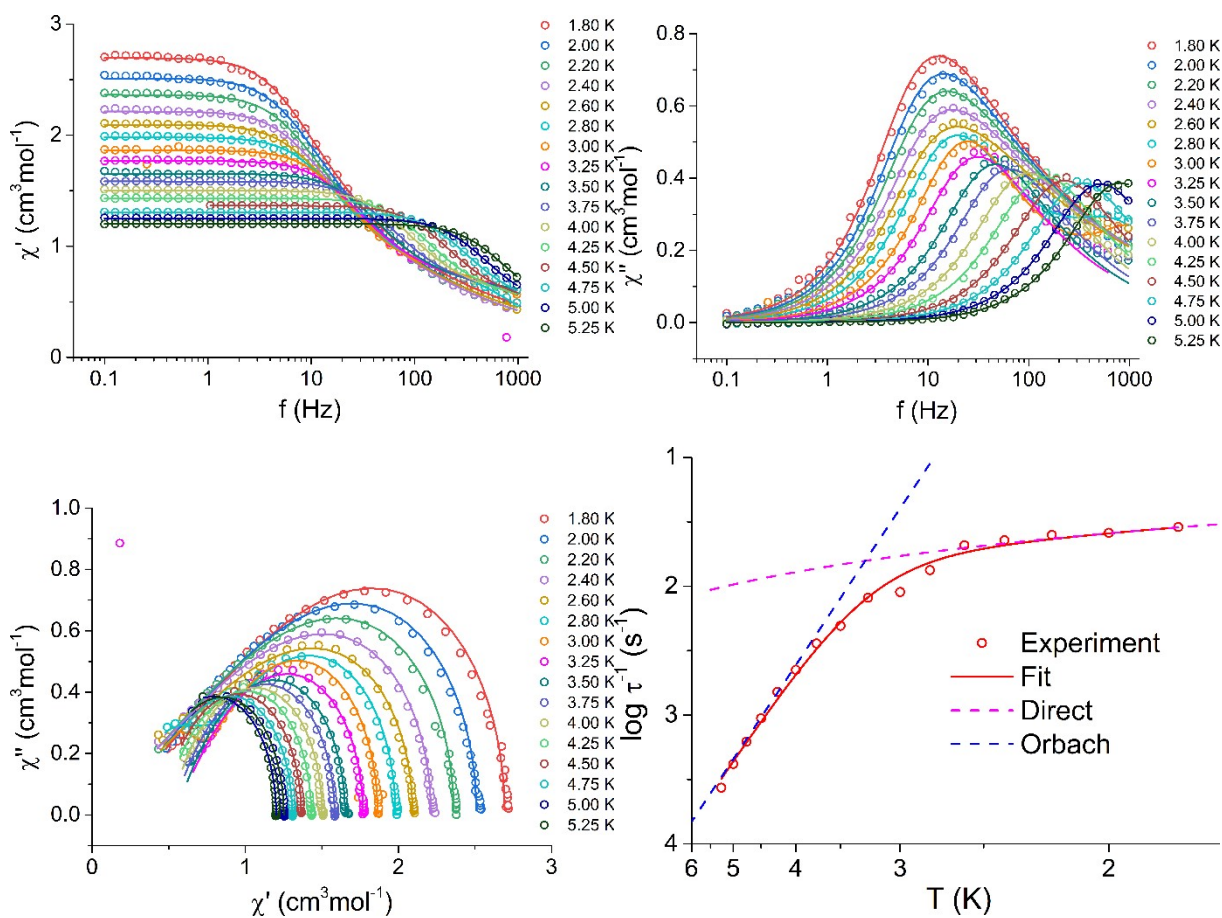


Figure S12. AC magnetic data and relaxation time fit for **2**, shown are dependences of in-phase and out-of-phase susceptibilities on frequency (upper left and right), Cole-Cole diagram (lower left) and fit of relaxation time (lower right).

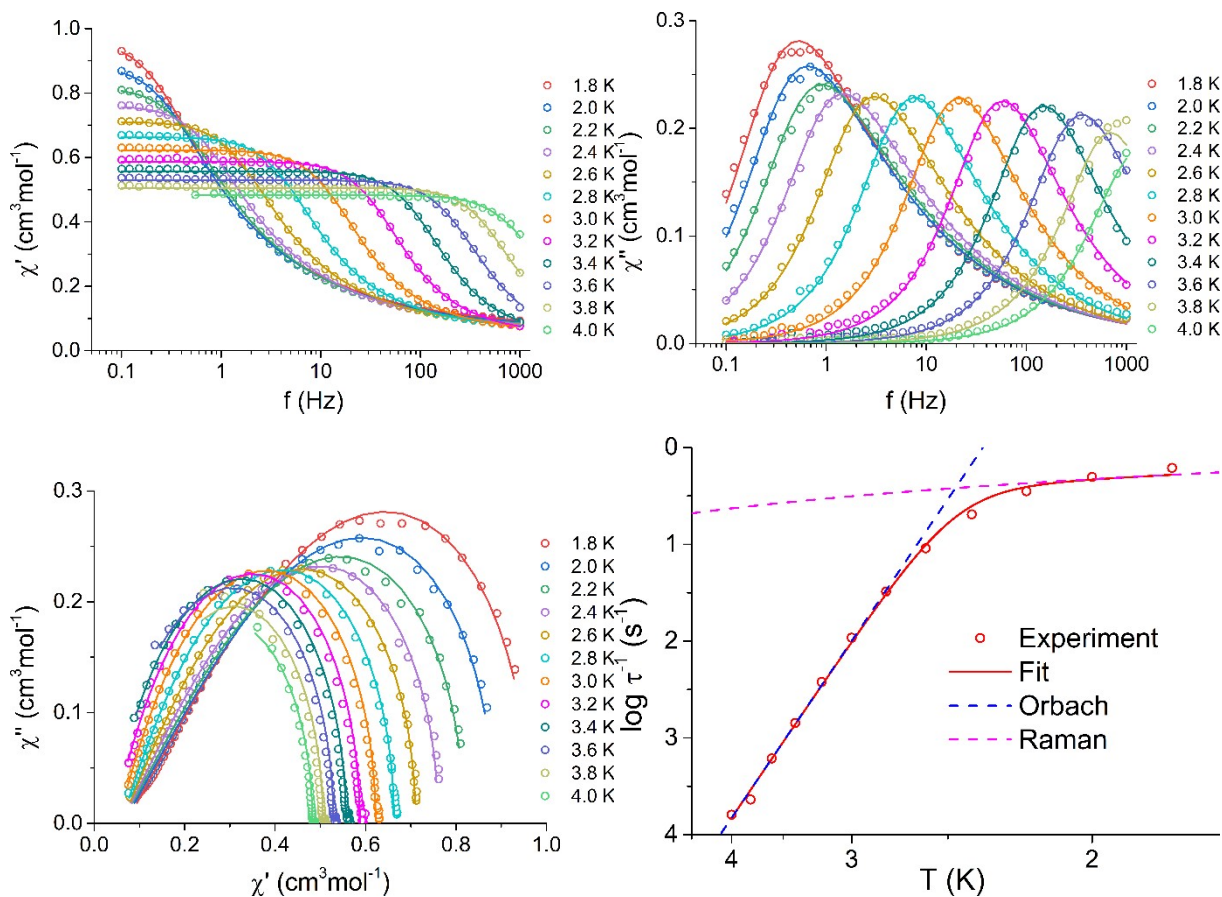


Figure S13. AC magnetic data and relaxation time fit for **3**, shown are dependences of in-phase and out-of-phase susceptibilities on frequency (upper left and right), Cole-Cole diagram (lower left) and fit of relaxation time (lower right).

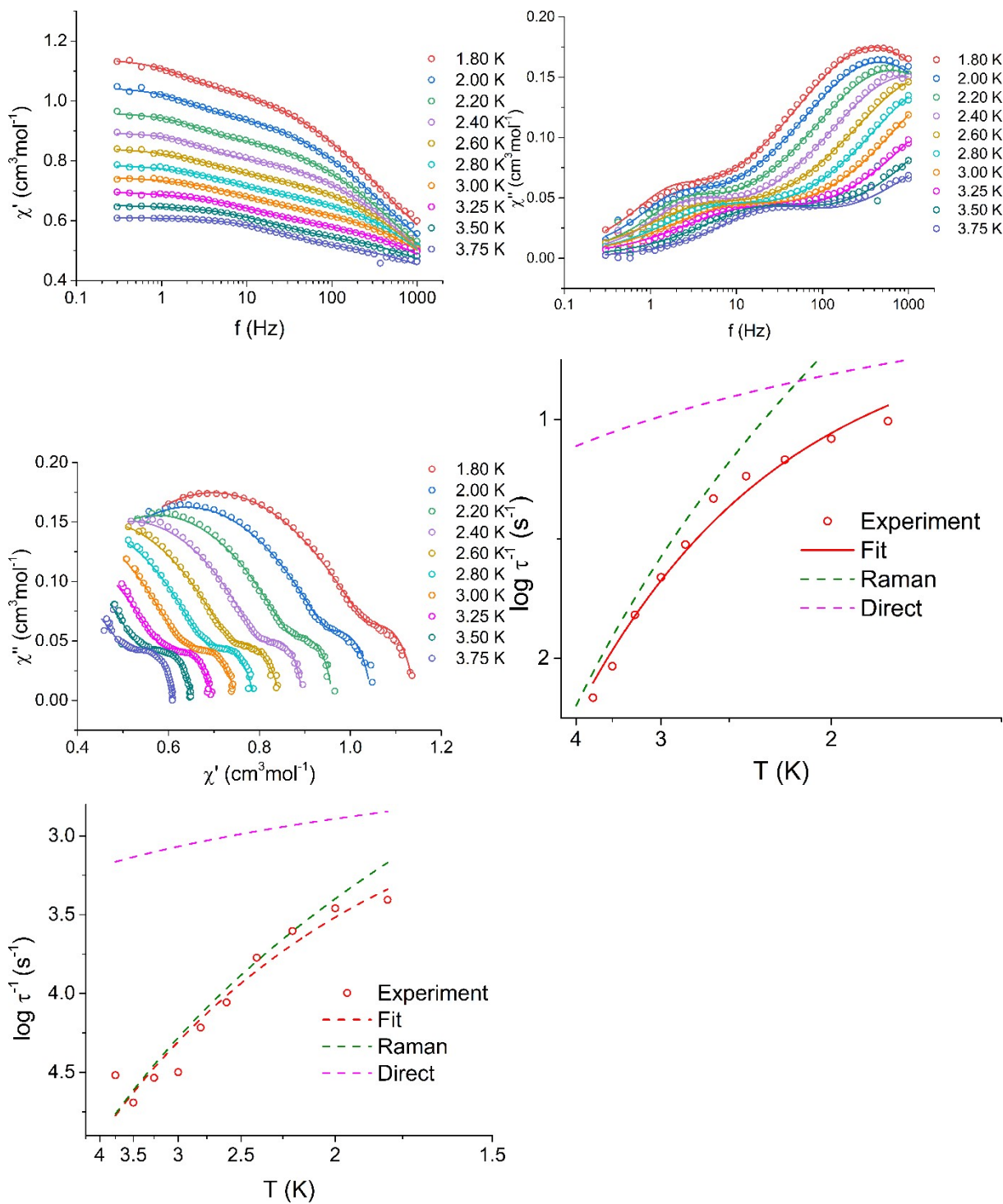


Figure S14. AC magnetic data and relaxation time fit for **5**, shown are dependences of in-phase and out-of-phase susceptibilities on frequency (upper left and right), Cole-Cole diagram (middle left) and fits of relaxation time (middle right and lower).

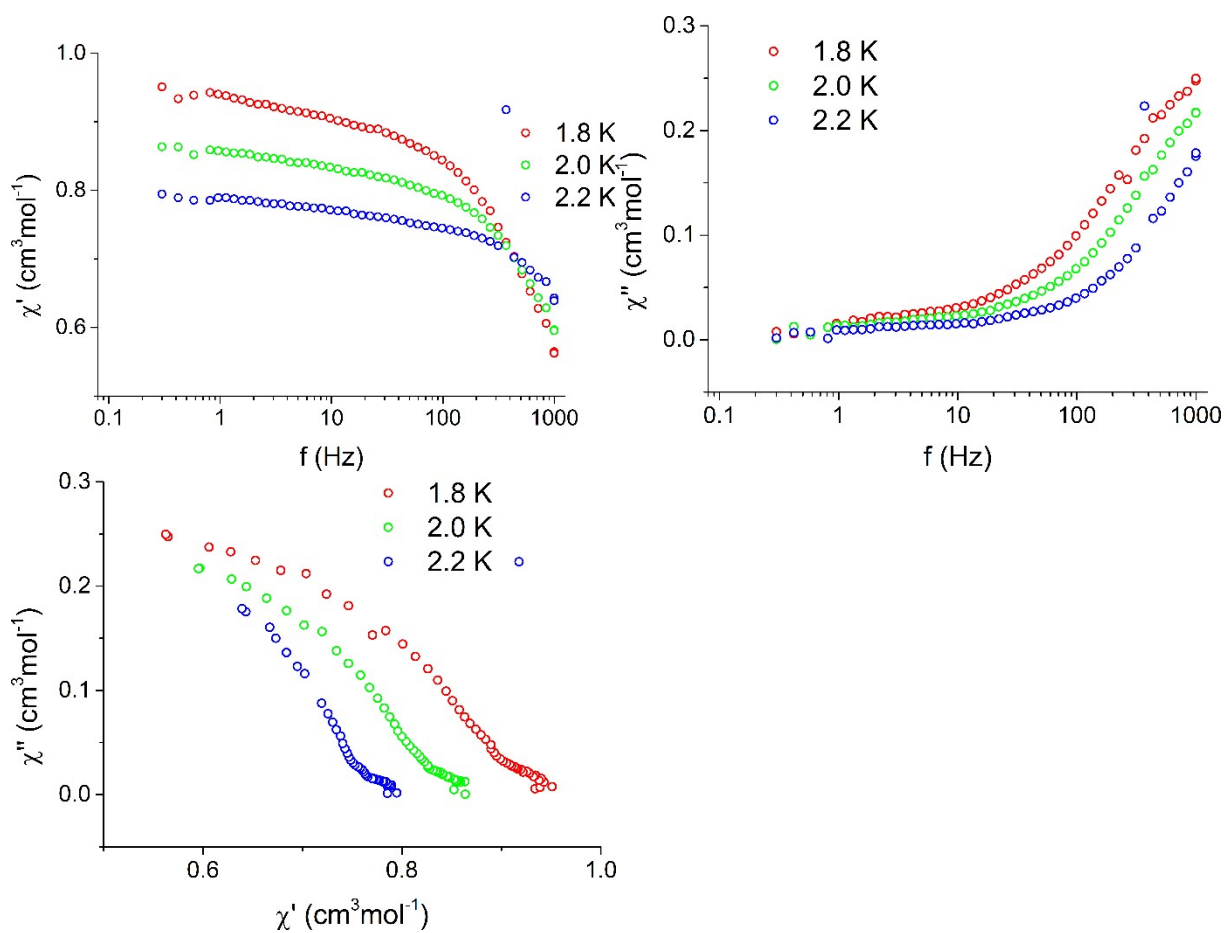


Figure S15: AC magnetic data for **6**, shown are dependences of in-phase and out-of-phase susceptibilities on frequency (upper left and right) and Cole-Cole diagram (lower).

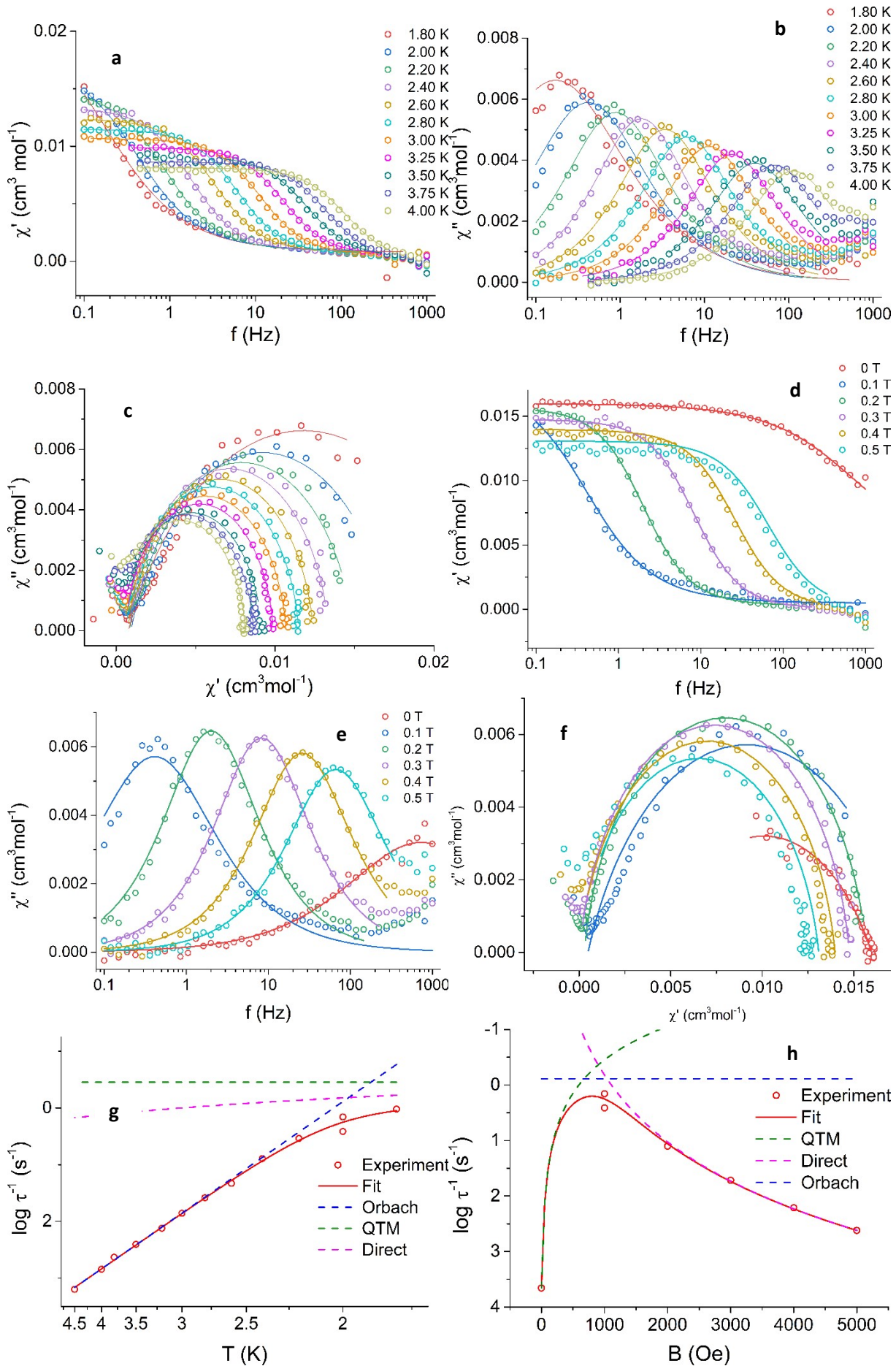


Figure S16: AC magnetic data for **1Zn**, shown are dependences of in-phase and out-of-phase susceptibilities on frequency for various temperatures and $B = 0.1$ T (**a** and **b**), Cole-Cole diagram for various temperatures and $B = 0.1$ T (**c**), dependences of in-phase and out-of-phase susceptibilities on frequency for various magnetic fields and $T = 2$ K (**d** and **e**), Cole-Cole diagram for various frequency for various magnetic fields and $T = 2$ K (**f**), and fits of relaxation time dependent on temperature (**g**) and magnetic field (**h**).

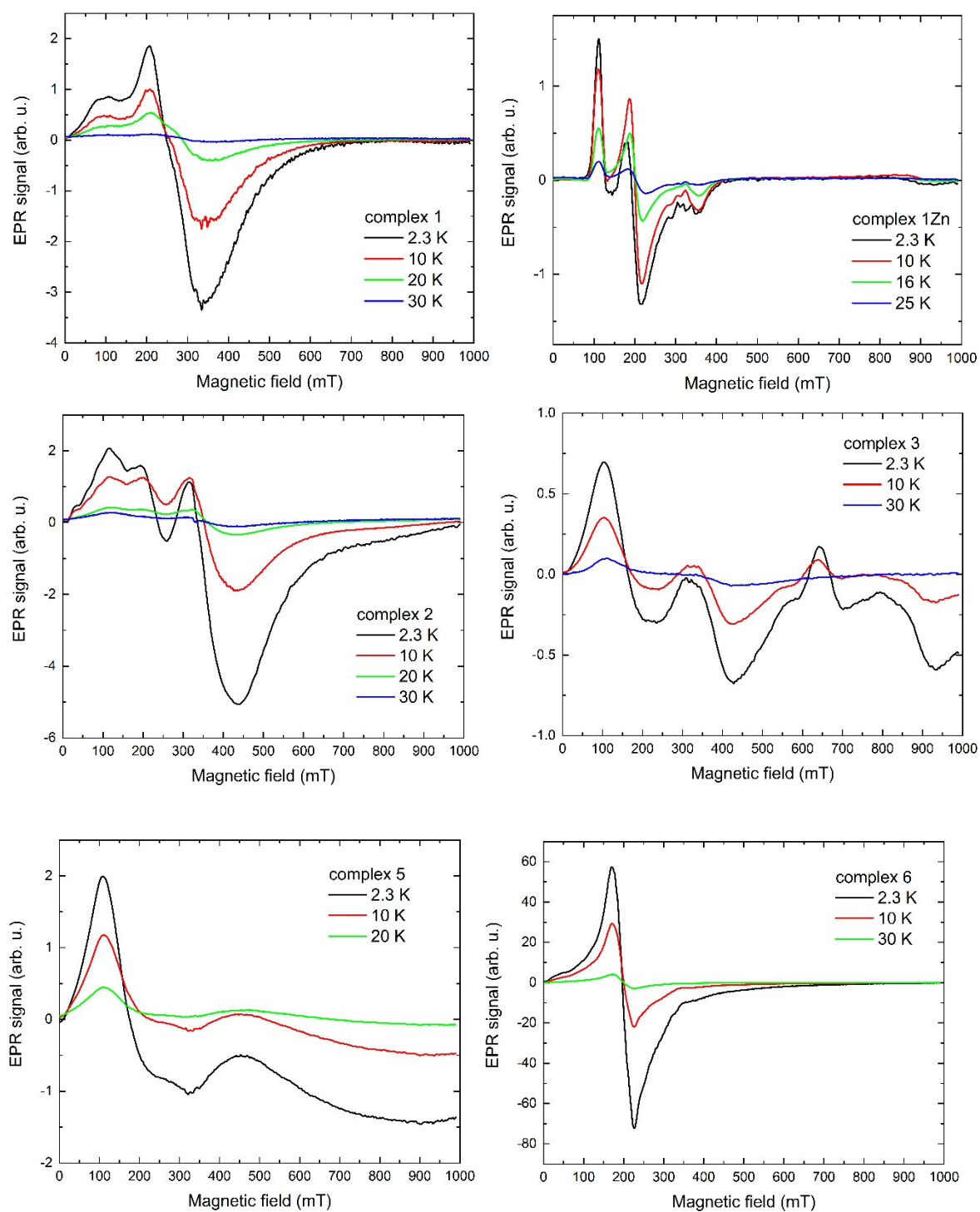


Figure S17: Thermal evolution of the powder X-band EPR spectra of **1**, **1Zn**, **2**, **3**, **5**, and **6**.

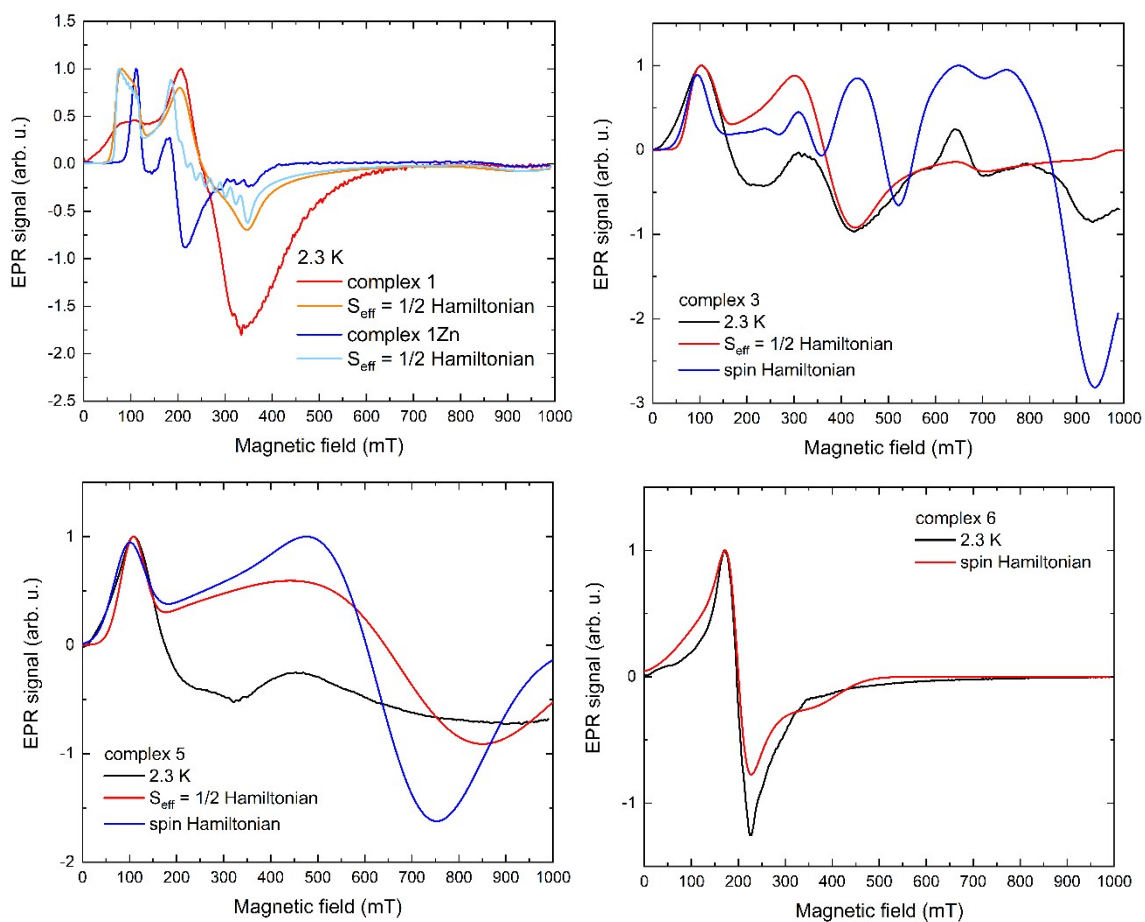
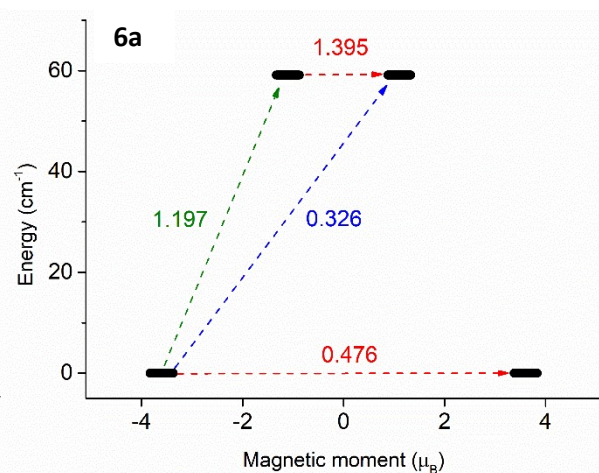
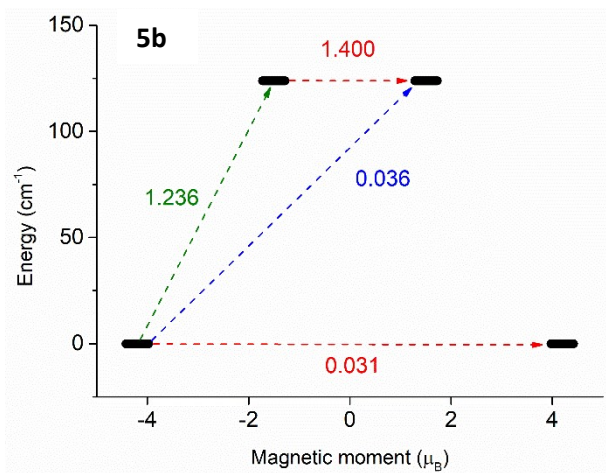
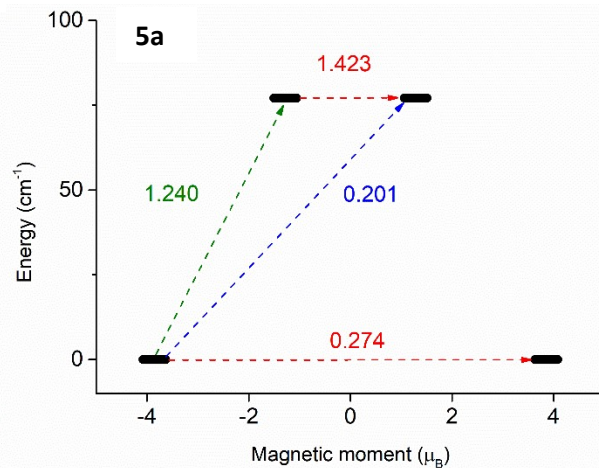
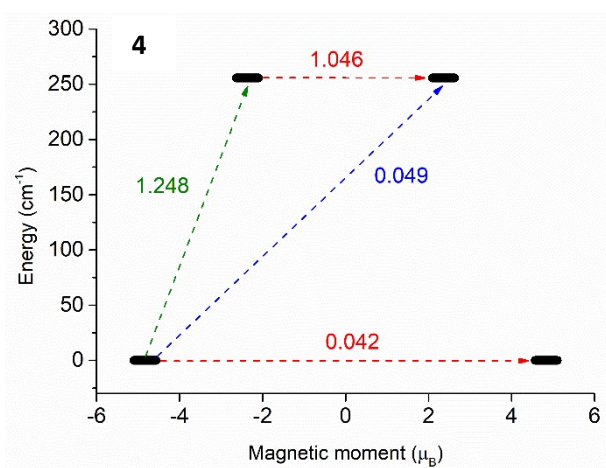
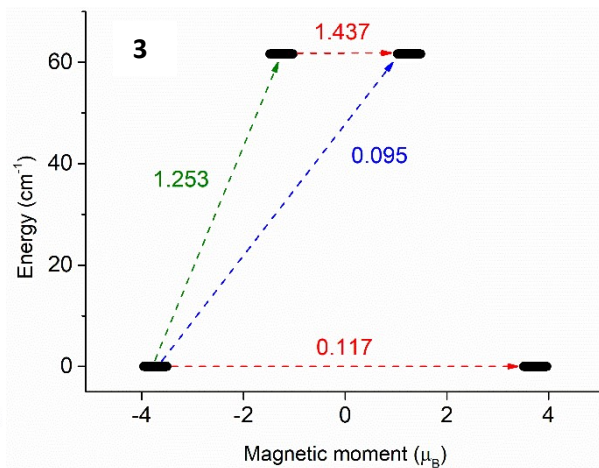
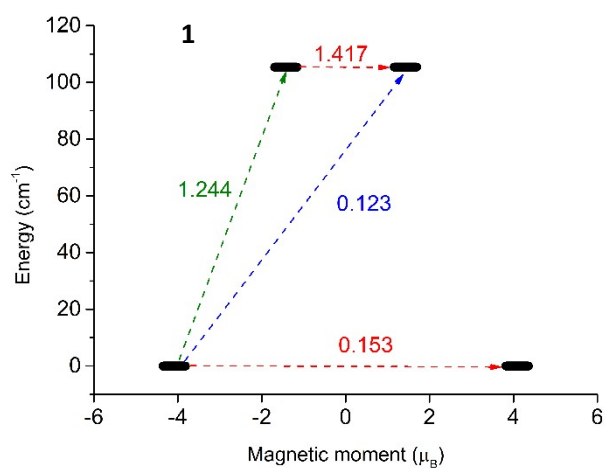


Figure S18. Simulations of the powder X-band EPR spectra of **1**, **1Zn**, **3**, **5**, and **6** obtained at 2.3 K using effective $S_{\text{eff}}=1/2$ Hamiltonian and spin Hamiltonian models.



6b

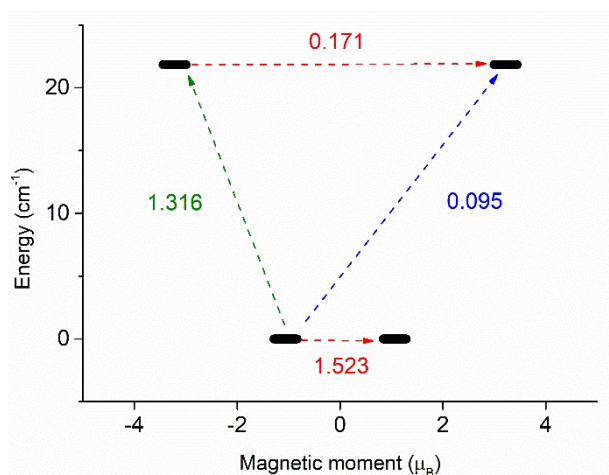


Figure S19. SINGLE_ANISO description of magnetic moment matrix elements between Kramer's doublets for studied complexes.

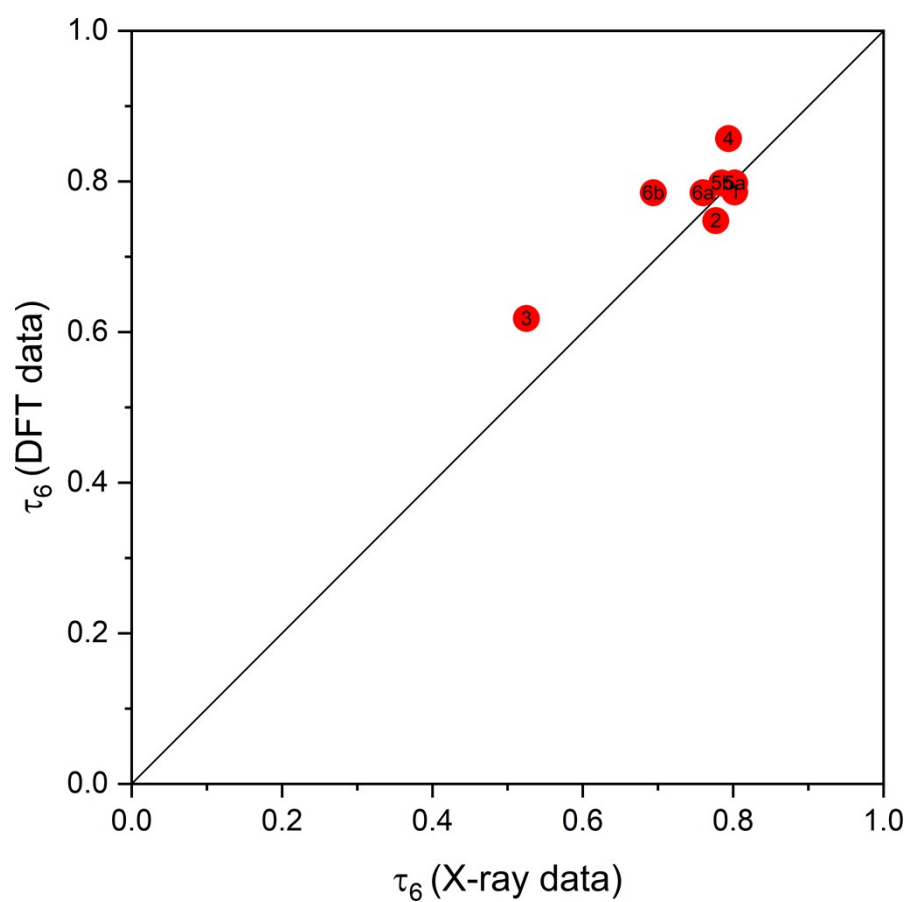


Figure S20. The comparison of structural parameter τ_6 calculated for **1-6** using X-ray data and data from DFT calculations.

Table S1. Detailed information about crystallographic experiments regarding 1-6

Identification code	1	2	3	4	5	6
Empirical formula	C ₂₁ H ₂₂ CoN ₂ O ₇	C ₂₆ H ₂₄ CoN ₂ O ₇ S	C ₂₂ H ₂₄ CoN ₂ O ₇	C ₂₂ H ₂₄ CoN ₂ O ₈	C ₄₉ H ₅₂ Co ₂ N ₄ O ₁₃	C ₃₂ H ₂₆ CoN ₂ O ₆
Formula weight	473.33	567.46	487.36	503.378	1022.845	593.506
Temperature/K	293(2)	293(2)	293(2)	293(2)	293(2)	293(2)
Crystal system	monoclinic	triclinic	triclinic	monoclinic	monoclinic	orthorhombic
Space group	P2 ₁ /c	P-1	P-1	P2 ₁ /n	P2 ₁ /n	lba2
a/Å	8.1602(2)	8.2410(2)	8.1468(2)	8.60879(9)	8.1786(1)	15.8026(5)
b/Å	18.3720(3)	9.8612(2)	9.7759(3)	18.86185(14)	40.6271(3)	31.8280(7)
c/Å	14.2319(2)	15.9236(4)	14.0873(3)	14.24696(13)	15.0552(1)	26.8107(9)
α/°	90	80.846(2)	93.491(2)	90	90	90
β/°	103.006(2)	82.025(2)	104.865(2)	107.5861(10)	103.388(1)	90
γ/°	90	84.8036(19)	93.594(2)	90	90	90
Volume/Å ³	2078.90(7)	1262.10(5)	1078.81(5)	2205.27(4)	4866.49(8)	13484.8(7)
Z	4	2	2	4	4	16
ρ _{calc} /cm ³	1.512	1.493	1.5	1.516	1.396	1.169
μ/mm ⁻¹	6.884	6.528	6.649	6.561	5.909	4.327
F(000)	980	586	506	1039	2117.8	4893.5
Crystal size/mm ³	0.25 × 0.18 × 0.15	0.3 × 0.28 × 0.23	0.24 × 0.18 × 0.15	0.34 × 0.28 × 0.22	0.25 × 0.22 × 0.11	0.32 × 0.24 × 0.22
Radiation	CuKα (λ = 1.54184)	CuKα (λ = 1.54184)	CuKα (λ = 1.54184)	Cu Kα (λ = 1.54184)	Cu Kα (λ = 1.54184)	Cu Kα (λ = 1.54184)
2θ range for data collection/°	7.988 to 136.7	5.668 to 139.826	6.512 to 139.766	8.02 to 136.42	4.34 to 136.58	5.56 to 136.88
Index ranges	-9 ≤ h ≤ 9, -21 ≤ k ≤ 21, -17 ≤ l ≤ 14	-10 ≤ h ≤ 10, -11 ≤ k ≤ 11, -19 ≤ l ≤ 19	-9 ≤ h ≤ 8, -11 ≤ k ≤ 11, -17 ≤ l ≤ 17	-10 ≤ h ≤ 10, -22 ≤ k ≤ 22, -17 ≤ l ≤ 17	-9 ≤ h ≤ 9, -48 ≤ k ≤ 48, -18 ≤ l ≤ 14	-17 ≤ h ≤ 19, -36 ≤ k ≤ 38, -32 ≤ l ≤ 32
Reflections collected	11709	39638	21859	75302	74278	34085
Independent reflections	3784 [R _{int} = 0.0301, R _{sigma} = 0.0309]	4706 [R _{int} = 0.0398, R _{sigma} = 0.0168]	4031 [R _{int} = 0.0415, R _{sigma} = 0.0209]	4042 [R _{int} = 0.0946, R _{sigma} = 0.0237]	8888 [R _{int} = 0.0392, R _{sigma} = 0.0177]	11039 [R _{int} = 0.0341, R _{sigma} = 0.0365]
Data/restraints/parameters	3784/0/283	4706/66/375	4031/0/291	4042/2/315	8888/0/615	11039/433/849
Goodness-of-fit on F ²	1.033	1.038	1.075	1.037	1.044	1.008
Final R indexes [I > 2σ (I)]	R ₁ = 0.0334, wR ₂ = 0.0836	R ₁ = 0.0296, wR ₂ = 0.0817	R ₁ = 0.0303, wR ₂ = 0.0826	R ₁ = 0.0371, wR ₂ = 0.1042	R ₁ = 0.0399, wR ₂ = 0.1060	R ₁ = 0.0568, wR ₂ = 0.1637
Final R indexes [all data]	R ₁ = 0.0414, wR ₂ = 0.0873	R ₁ = 0.0304, wR ₂ = 0.0822	R ₁ = 0.0321, wR ₂ = 0.0843	R ₁ = 0.0410, wR ₂ = 0.1070	R ₁ = 0.0438, wR ₂ = 0.1085	R ₁ = 0.0825, wR ₂ = 0.1863
Largest diff. peak/hole / e Å ⁻³	0.20/-0.22	0.27/-0.31	0.23/-0.33	0.25/-0.49	0.70/-0.33	0.25/-0.28
Flack Parameter						-0.0207(16)
CCDC	2288033	2288038	2288037	2288035	2288036	2288034

Table S2: Uncertainties of best-fitted parameters from DC magnetic measurements (Table 3)

	g_{xy}	g_z / g_{iso}	D	E	TIP
1	0.00253	0.00151	0.264	0.121	-
2	-	0.00140	0.0886	0.0677	0.0000164
3	0.00223	0.00196	0.121	0.0749	$0.133 \cdot 10^{-4}$
5	0.00599	0.00274	0.418	0.150	0.0000372
6	0.00215	0.00798	0.149	0.0453	0.0000137

Table S3. AC magnetic data fit parameters for **1**

T	α_1	β_1	$\log \tau_1$	$X_{T1}-\chi_s$	X_s	α_2	β_2	$\log \tau_2$	$X_{T2}-\chi_s$
1.8	0.15743	0.39907	-0.95249	1.15785	0.11142	0	1	0	0
2.0	0.12288	0.34753	-0.99561	1.07191	0.07763	0	1	0	0
2.2	0.18966	0.48293	-1.21892	0.87855	0.05831	0	1	-3.51585	0.06417
2.4	0.18448	0.62777	-1.43251	0.71522	0.06887	0	1	-3.66873	0.11795
2.6	0.1678	0.59356	-1.50122	0.66434	0.06381	0	1	-3.99495	0.10614
2.8	0.18566	0.57969	-1.57864	0.63409	0.20835	0	1	0	0
3.0	0.15564	0.56437	-1.6518	0.58415	0.20151	0	1	0	0
3.25	0.13789	0.57616	-1.78043	0.53355	0.19289	0	1	0	0
3.5	0.1272	0.58571	-1.90715	0.49564	0.18138	0	1	0	0
3.75	0.11078	0.5988	-2.04708	0.4609	0.1725	0	1	0	0
4.0	0.0819	0.59512	-2.17799	0.43193	0.16348	0	1	0	0
4.25	0.06509	0.61682	-2.33717	0.40482	0.15725	0	1	0	0
4.5	0	0.5785	-2.45395	0.38065	0.14936	0	1	0	0
5.0	0	0.62672	-2.78637	0.34706	0.13424	0	1	0	0
5.5	0	0.63564	-3.09124	0.32729	0.11376	0	1	0	0
6.0	0	0.62308	-3.37087	0.31804	0.08885	0	1	0	0
6.5	0	1	-3.74468	0.23961	0.13838	0	1	0	0

Table S4. AC magnetic data fit parameters for **2**

T	α_1	β_1	$\log \tau_1$	$X_{T1}-X_S$	X_S	α_2	β_2	$\log \tau_2$	$X_{T2}-X_S$
1.8	0	0.35509	-1.54067	2.55693	0.13658	0	1	0	0
2.0	0	0.35004	-1.58582	2.40659	0.10261	0	1	0	0
2.2	0	0.33193	-1.60262	2.31453	0.04694	0	1	0	0
2.4	0	0.31942	-1.64342	2.18147	0.0306	0	1	0	0
2.6	0	0.311	-1.68245	2.04212	0.05011	0	1	0	0
2.8	0	0.5503	-1.87538	1.37033	0.12473	0	1	-3.70426	0.36057
3.0	0	0.67532	-2.04511	1.19313	0.10516	0	1	-3.90593	0.42237
3.25	0	0.55044	-2.08944	1.23306	0.53504	0	1	0	0
3.5	0	0.6188	-2.3086	1.107	0.54421	0	1	0	0
3.75	0	0.61945	-2.44497	1.07217	0.51068	0	1	0	0
4.0	0	0.66059	-2.64933	1.01073	0.49105	0	1	0	0
4.25	0	0.65951	-2.81994	0.98572	0.44474	0	1	0	0
4.5	0	0.69139	-3.02563	0.93759	0.42743	0	1	0	0
4.75	0	0.69657	-3.20692	0.91901	0.38688	0	1	0	0
5.0	0	0.67721	-3.37999	0.92383	0.32735	0	1	0	0
5.25	0	0.66094	-3.56413	0.94252	0.25885	0	1	0	0

Table S5. AC magnetic data fit parameters for **3**

T	α	β	$\log \tau$	X_T-X_S	X_S
1.8	0	0.40947	-0.21122	0.89291	0.0701
2.0	0	0.40768	-0.30431	0.82066	0.06444
2.2	0	0.41644	-0.45242	0.75666	0.06063
2.4	0	0.44729	-0.69117	0.69961	0.06069
2.6	0	0.49946	-1.04132	0.64993	0.0606
2.8	0	0.56565	-1.48849	0.60471	0.0581
3.0	0	0.62681	-1.9652	0.57108	0.05104
3.2	0	0.66589	-2.42175	0.54686	0.04027
3.4	0	0.69056	-2.84618	0.52598	0.03059
3.6	0	0.66092	-3.21204	0.51802	0.01096
3.8	0	0.98591	-3.63586	0.39492	0.11063
4.0	0	0.56977	-3.79365	0.4824	2.68E-10

Table S6. AC magnetic data fit parameters for **5**

T	α_1	β_1	$\log \tau_1$	$X_{T1-\chi_S}$	X_S	α_2	β_2	$\log \tau_2$	$X_{T2-\chi_S}$
1.8	0.45994	1	-3.40604	0.77239	1.55E-01	0	1	-1.00684	0.06307
2.0	0.44598	1	-3.45911	0.69819	1.45E-01	--	1	-1.08045	0.06022
2.2	0.44066	1	-3.60351	0.6614	1.22E-01	--	1	-1.16829	0.05848
2.4	0.43445	1	-3.77256	0.63134	1.01E-01	--	1	-1.23731	0.06299
2.6	0.43923	1	-4.05592	0.63727	6.27E-02	0.21007	1	-1.33094	0.08307
2.8	0.43923	1	-4.05592	0.63727	6.27E-02	0.21007	1	-1.33094	0.08307
3.0	0.4203	1	-4.49915	0.61385	1.71E-02	0.27754	1	-1.66086	0.10093
3.25	0.40452	1	-4.53427	0.49682	4.98E-02	0.29147	1	-1.81822	0.10219
3.5	0.40452	1	-4.53427	0.49682	4.98E-02	0.29147	1	-1.81822	0.10219
3.75	0.38162	1	-4.518	0.33584	9.60E-02	0.17751	1	-2.16437	0.08679

Table S7. AC magnetic data fit parameters for **1Zn**

T	B (T)	α	β	$\log \tau$	$X_T-\chi_S$	X_S
1.8	0.1	0.304	1	-0.01995	0.02213	8.73E-04
2	0.1	0	0.51229	-0.15861	0.01482	4.68E-04
2.2	0.1	0	0.65441	-0.53822	0.01378	6.09E-04
2.4	0.1	0	0.73823	-0.89159	0.01254	6.14E-04
2.6	0.1	0.08176	1	-1.3301	0.01145	8.98E-04
2.8	0.1	0.05103	1	-1.58311	0.01055	8.56E-04
3	0.1	0.09202	1	-1.8575	0.01017	5.43E-04
3.2	0.1	0.06498	1	-2.12234	0.00931	5.75E-04
3.5	0.1	0.07249	1	-2.40501	0.00874	3.32E-04
3.8	0.1	0.07594	1	-2.63151	0.0086	4.54E-05
4	0.1	0.06419	1	-2.84391	0.00796	9.89E-05
4.5	0.1	0.02289	1	-3.19895	0.00721	0
2	0	0.36315	1	-3.65785	0.01174	0.00423
2	0.1	0.25663	1	-0.41357	0.01731	4.88E-04
2	0.2	0.11209	1	-1.1027	0.01543	2.81E-04
2	0.3	0.1035	1	-1.71886	0.01474	1.81E-05
2	0.4	0.11563	1	-2.21218	0.01397	0
2	0.5	0.12798	1	-2.6195	0.01308	0

Table S8. CASSCF/NEVPT2 calculated *g*-factors of Kramers doublets for studied complexes **1-6**

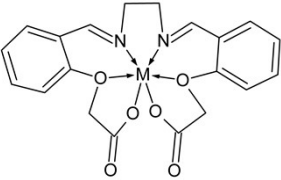
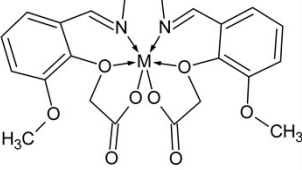
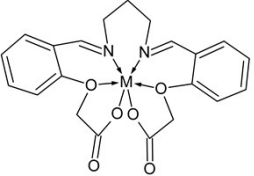
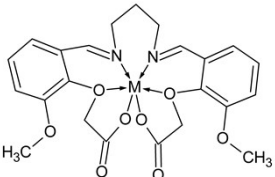
	KD 1 gx	KD 1 gy	KD 1 gz	KD 2 gx	KD 2 gy	KD 2 gz
1	0.4333	0.4864	8.1751	4.6026	3.9010	2.8479
2	0.3077	0.3269	7.7574	4.5538	4.0276	2.6437
3	0.3461	0.3562	7.4724	4.6310	3.9966	2.5102
4	0.1278	0.1432	9.7381	2.7767	2.8593	5.0354
5a	0.7482	0.8985	7.7102	2.5657	3.5760	4.9628

5b	0.0899	0.0939	8.3966	4.2587	4.1411	3.0052
6a	1.2178	1.6407	7.2067	2.2042	2.9257	5.4484
6b	5.0955	4.0418	2.1232	0.5006	0.5224	6.4332

Table S9. Selected structural parameters along with CSM and τ_6 shape analysis of DFT optimized molecular structures for **1-6** with the help of B3LYP functional

	Co – N1	Co – N2	Co – O1	Co – O2	Co – O3	Co – O4	CSM TP	CSM OH	τ_6
1	2.0902	2.0904	1.9533	2.3854	2.3873	1.9533	2.134	16.890	0.786
2	2.0766	2.0779	1.9557	2.3717	2.3709	1.9563	2.783	15.059	0.748
3	2.0996	2.0976	1.9742	2.377	2.3795	1.9706	3.690	8.674	0.618
4	2.118	2.1178	1.9534	2.4081	2.4274	1.9481	1.586	16.176	0.857
5	2.0808	2.0797	1.9594	2.3677	2.3649	1.9597	1.777	16.287	0.798
6	2.0759	2.0794	1.9536	2.3789	2.382	1.9664	2.099	16.533	0.785

Table S10. The comparison of Continuous Shape Measures for complexes reported in CSD.^a

Structural motif	
	1 (CSM ^{TP} = 1.631, CSM ^{OH} = 16.812) M = Zn, MELYAE ¹ (CSM ^{TP} = 2.262, CSM ^{OH} = 17.871) M = Zn, VUQCEQ ² (CSM ^{TP} = 1.903&1.926, CSM ^{OH} = 17.419&17.263)
	M = Co, RUJNES ³ (CSM ^{TP} = 5.540, CSM ^{OH} = 5.212) M = Zn, SIRMUX ⁴ (CSM ^{TP} = 7.036, CSM ^{OH} = 6.808)
	3 (CSM ^{TP} = 4.727, CSM ^{OH} = 5.626) M = Zn, HOMFIZ ⁵ (CSM ^{TP} = 2.299, CSM ^{OH} = 11.719) M = Co, HOMFOF ⁶ (CSM ^{TP} = 10.646, CSM ^{OH} = 1.533)
	M = Ni, QEBBIL ⁷ (CSM ^{TP} = 14.001, CSM ^{OH} = 0.622) M = Zn, SIRMUD ⁴ (CSM ^{TP} = 10.706, CSM ^{OH} = 1.551)

^a CSM^{TP} = continuous shape measure for trigonal prism shape; CSM^{OH} = continuous shape measure for octahedron shape.

¹ Wang, J.; Zhu, D.-S.; Shao, K.-Z.; Xu, L. {2,2'-[Ethane-1,2-Diylbis(Nitrilomethylidene)]Diphenoxyacetato}zinc(II) Methanol Solvate. *Acta Crystallogr. Sect. E Struct. Reports Online* **2006**, 62 (8), m1884–m1886. <https://doi.org/10.1107/S1600536806026791>.

² Yang X., Wang J., Han L., *Dongbei Shi-Daxuebao Ziran Kexueban*, 2007, 39, 72-1

³ Yan, L.; Liu, W.; Wang, M. J.; Xu, Y.; Shi, K. Z. Synthesis, Characterization, Oxygen Respiratory, Antibacterial Activity, and Photoluminescent Property Studies of One Novel Complex with Schiff-Base Ligand. *Jiegou Huaxue* **2020**, 39 (5), 895–900. <https://doi.org/10.14102/J.CNKI.0254-5861.2011-2585>.

- ⁴ Yan, L.; Wang M.-J. Synthesis, Crystal Structures and Fluorescence of Two Zn(II) Complexes with Schiff Base Ligands. *Chinese Journal of Inorganic Chemistry*. 2013, **29**(11), 2370-2374. <https://doi.org/10.3969/j.issn.1001-4861.2013.00.351>
- ⁵ Wang, Z. L.; Zhu, D. S.; Wang, R. S. Crystal Structure of [N,N'-(Bis(2-Phenoxyacetic)Formylidene)Propane-1,3-Diamine-Zinc(II)] - Water - Ethanol (1:1:0.25), [Zn(C₂₁H₂₀N₂O₆)]·H₂O·0.25C₂H₆O. *Zeitschrift fur Krist. - New Cryst. Struct.* **2008**, **223** (3), 215–216. <https://doi.org/10.1524/NCRS.2008.0090/DOWNLOADASSET/1267-2227.CFF>.
- ⁶ Wang, Z. L.; Zhu, D. S.; Wang, R. S. Crystal Structure of [N,N'-(Bis(2-Phenoxyacetic)Formylidene)Propane-1,3-Diaminecobalt(II)] Hexahydrate, [Co(C₂₁H₂₀N₂O₆)]·6H₂O. *Zeitschrift fur Krist. - New Cryst. Struct.* **2008**, **223** (3), 217–218. <https://doi.org/10.1524/NCRS.2008.0091>
- ⁷ Yan, L.; Liu, C. L. Synthesis, Structure Characterization, Antibacterial Activity and Fluorescence Studies of a Ni(II) Compound with Schiff-Base Ligand. *Jiegou Huaxue* 2017, **36** (8), 1315–1320. <https://doi.org/10.14102/J.CNKI.0254-5861.2011-1522>.